Kinetics and mechanism of amyloid formation by the prion protein H1 peptide as determined by time-dependent ESR

Karen M Lundberg[1], Chris J Stenland[1], Fred E Cohen[2], Stanley B Prusiner[3] and Glenn L Millhauser[1]

Background: Peptides derived from three of four putative α-helical regions of the prion protein (PrP) form amyloid in solution. These peptides serve as models for amyloidogenesis and for understanding the α helix→β strand conformational change that is responsible for the development of disease. Kinetic studies of amyloid formation usually rely on the detection of fibrils. No study has yet explored the rate of monomer peptide uptake or the presence of nonfibrillar intermediate species. We present a new electron spin resonance (ESR) method for probing the kinetics of amyloid formation. A spin label was covalently attached to a highly amyloidogenic peptide and kinetic trials were monitored by ESR.

Results: Electron microscopy shows that the spin-labeled peptide forms amyloid, and ESR reveals the kinetic decay of free peptide monomer during amyloid formation. The combination of electron microscopy and ESR suggests that there are three kinetically relevant species: monomer peptide, amyloid and amorphous aggregate (peptide aggregates devoid of fibrils or other structures with long-range order). A rather surprising result is that amyloid formation requires the presence of this amorphous aggregate. This is particularly interesting because PrP^{Sc}, the form of PrP associated with scrapie, is often found as an aggregate and amyloid formation is not a necessary component of prion replication or pathogenesis.

Conclusions: Kinetic analysis of the time-dependent data suggests a model whereby the amorphous aggregate has a previously unsuspected dual role: it releases monomer into solution and also provides initiation sites for fibril growth. These findings suggest that the β-sheet-rich PrP^{Sc} may be stabilized by aggregation.

Addresses: [1]Department of Chemistry and Biochemistry, University of California, Santa Cruz, CA 95064, USA. [2]Departments of Medicine, Pharmacology, and Biochemistry and Biophysics, University of California, San Francisco, CA 94143, USA. [3]Departments of Neurology, and Biochemistry and Biophysics, University of California, San Francisco, CA 94143, USA.

Correspondence: Glenn L Millhauser
E-mail: glennm@chemistry.ucsc.edu

Key words: aggregation, amyloid, electron spin resonance, kinetics, prion protein

Received: **26 February 1997**
Accepted: **26 March 1997**

Chemistry & Biology May 1997, **4**:345–355
http://biomednet.com/elecref/1074552100400345

Introduction

Prion diseases include scrapie (in sheep), bovine spongiform encephalopathy (mad cow disease), and the human diseases fatal familial insomnia, Creutzfeldt–Jakob disease, Gerstmann–Sträussler–Scheinker disease and kuru [1–4]. The scrapie isoform of the prion protein (PrP^{Sc}) is so named because it appears to be the sole macromolecule that is responsible for transmission of prion diseases. The normal cellular PrP isoform (PrP^{C}) is produced primarily in healthy tissue of the central nervous system. In prion diseases, PrP^{Sc} accumulates. This isoform has the same primary structure as PrP^{C} but a different tertiary structure. The conversion of PrP^{C} into PrP^{Sc} involves a binding event between existing PrP^{Sc} and PrP^{C} [2,5] and recent studies show that PrP^{Sc} functions as a template for this structural transition [6].

Circular dichroism and Fourier transform infrared spectroscopy have been used to investigate the secondary structure of PrP^{C} and PrP^{Sc} [7–9]. Both species have been isolated under non-denaturing conditions. The cellular form was found to contain 42% α helix and 3% β sheet [8]; in contrast, PrP^{Sc} has an α-helix content of 30% and a β-sheet content of 43%. Spectroscopic studies on PrP-derived peptides support these findings [10,11]. Thus, a protein refolding transition involving α helix→β sheet is implicated in the interconversion of PrP^{C} to PrP^{Sc}.

F.E.C., S.B.P. and coworkers [12] proposed a model in which PrP^{C} possesses four α-helical regions. Nuclear magnetic resonance (NMR) studies of PrP(90–145) supports the existence of the first of these α-helical regions [10] and an NMR structure of PrP(121–231) documents the existence of the third and fourth α-helical regions [13]. Of the 13 disease-causing point mutations, 12 are found in or near the regions of secondary structure. Peptides derived from three of the experimentally documented α helices have been shown to form amyloid that exhibits the same birefringence and electron microscopy features as observed in some prion diseases, Alzheimer's disease and the other amyloidoses [14]. The peptide sequence AGAAAAGA, corresponding to residues 113–120 from Syrian hamster PrP, a part of the H1 region, is of particular interest. This

sequence is the most amyloidogenic fragment derived from PrP and is conserved in all known PrP sequences [15]. Also, the Ala117→Val mutation that segregates with Gerstmann–Sträussler–Scheinker disease is found within this sequence [16]. A molecular model, which takes into account both the spectroscopic observations and the sites of disease-associated mutations, suggests that this sequence forms part of a β sheet in PrP^{Sc} [17].

Although the formation of amyloid is not a necessary consequence of prion disease, multimerization of monomeric units is thought to be an essential component of PrP^{Sc} replication. Thus, it is important to understand how conformationally plastic regions of PrP can associate to form ordered aggregates. Fibrils that are characteristic of amyloid are composed largely of β sheet [18]. Hence, amyloid formation may provide an insight into the rate at which PrP-derived peptides rearrange into extended β-sheet conformations. In addition, PrP^{Sc} can, upon proteolytic cleavage near residue 90 and addition of detergent, form prion rods which have been shown to be amyloid on the basis of ultrastructural and tinctorial criteria [19,20]. Finally, short fibril-forming peptides can serve as useful models for amyloidogenesis, which is central to diseases such as Alzheimer's [21].

It is widely recognized that *in vitro* kinetic studies provide an insight into the mechanism responsible for the formation of amyloid. To date, most kinetics measurements have relied upon the time-dependent detection of extended fibrils. For example, Come *et al.* [22] used solution turbidity as a means of assessing fibril concentration in samples containing PrP-derived peptides. They demonstrated a kinetic lag time similar to that observed in crystal growth. Lomakin *et al.* [23] recently investigated the growth of β-amyloid peptide fibrils by quasielastic light scattering. The authors proposed a kinetic model in which peptide micelles rearrange to form a nascent fibril that subsequently elongates upon the attachment of peptide from solution. Although such experiments are essential, they cannot reveal complete descriptions of the kinetic processes responsible for the development of amyloid. Detailed kinetic studies require the identification of all the species present in solution. Experiments that detect only fibril concentration and/or growth cannot address important issues such as the rate law associated with the uptake of the monomeric peptide or the presence of intermediate species such as dimers or trimers. Such information would be vital for determining which of the proposed prion replication mechanisms actually occurs.

To address these issues, we present electron spin resonance (ESR) and electron microscopy (EM) experiments on a spin-labeled analog of the PrP(113–120) sequence AGAAAAGA. The peptide AGAACAGA [denoted PrP(113–120)–5] was synthesized and a nitroxide spin label was covalently attached to the cysteine residue. The resulting spin-labeled analog [PrP(113–120)–5SL] forms amyloid that is similar to that of the parent sequence. The spin-label reporter group is detectable by ESR down to micromolar concentrations. Monomeric peptide and aggregated species give distinct ESR signals, allowing each to be followed independently during amyloid formation. EM is used to assess the development of fibrils. By combining ESR and EM, three species are identified: monomeric peptide; amorphous aggregate that does not contain amyloid; and amyloid. We find no evidence for the presence of low molecular weight multimeric species such as dimers or trimers. ESR is also used in combination with a filtering experiment to explore kinetic reversibility. A three-state kinetic model that is consistent with the experimental results is proposed. A key feature of this model is the previously unsuspected dual role of the amorphous aggregate. This species releases peptide into solution and also provides sites for the initiation of amyloid growth.

Results

Spin-labeled peptides form amyloid

Amyloid formed readily from buffered solutions of PrP(113–120), PrP(113–120)–5 and PrP(113–120)–5SL after 2–3 days, as determined by transmission EM. The fibrils were at least 3 μm long and ~6–8 nm wide for each sample, as shown in Figure 1. Fibrils from the parent PrP(113–120) peptide had periodic twists whereas fibrils from the unlabeled and labeled analogs were straight. All fibrils were unbranched. The spin-labeled fibrils were stained with Congo Red (Sigma) and exhibited the green–gold birefringence that is characteristic of amyloid. Thus, PrP(113–120)–5SL retains the fibril-forming characteristics of the parent PrP(113–120) peptide.

ESR spectra exhibit time-dependent characteristics

To initiate each ESR-detected kinetic trial, measured amounts of PrP(113–120)–5SL were mixed with buffer and agitated to aid dissolution. ESR measurements were commenced within 5 min. Figure 2a shows two ESR spectra of PrP(113–120)–5SL taken from a single sample at 5 min and 2 h after dissolution. The sharp three-line first-derivative spectrum is characteristic for a rapidly tumbling, monomeric nitroxide-labeled peptide in solution. The rotational correlation time τ_R for this peptide, as determined from the spectra, is 0.15 ns which is the expected value for a monomeric peptide possessing the molecular weight of PrP(113–120)–5SL at 298K [24]. The center line is expanded to show clearly the loss of amplitude for the 2 h spectrum. Comparison of the two spectra shows that, as time progresses, the concentration of free peptide decays.

Figure 2b shows the same data as Figure 2a, but with the spectra displayed in the ESR absorption mode. In this representation, a broad spectral component can be seen, underlying the sharp three-line nitroxide spectrum. Passing PrP(113–120)–5SL solutions through a 0.22 μm filter

Figure 1

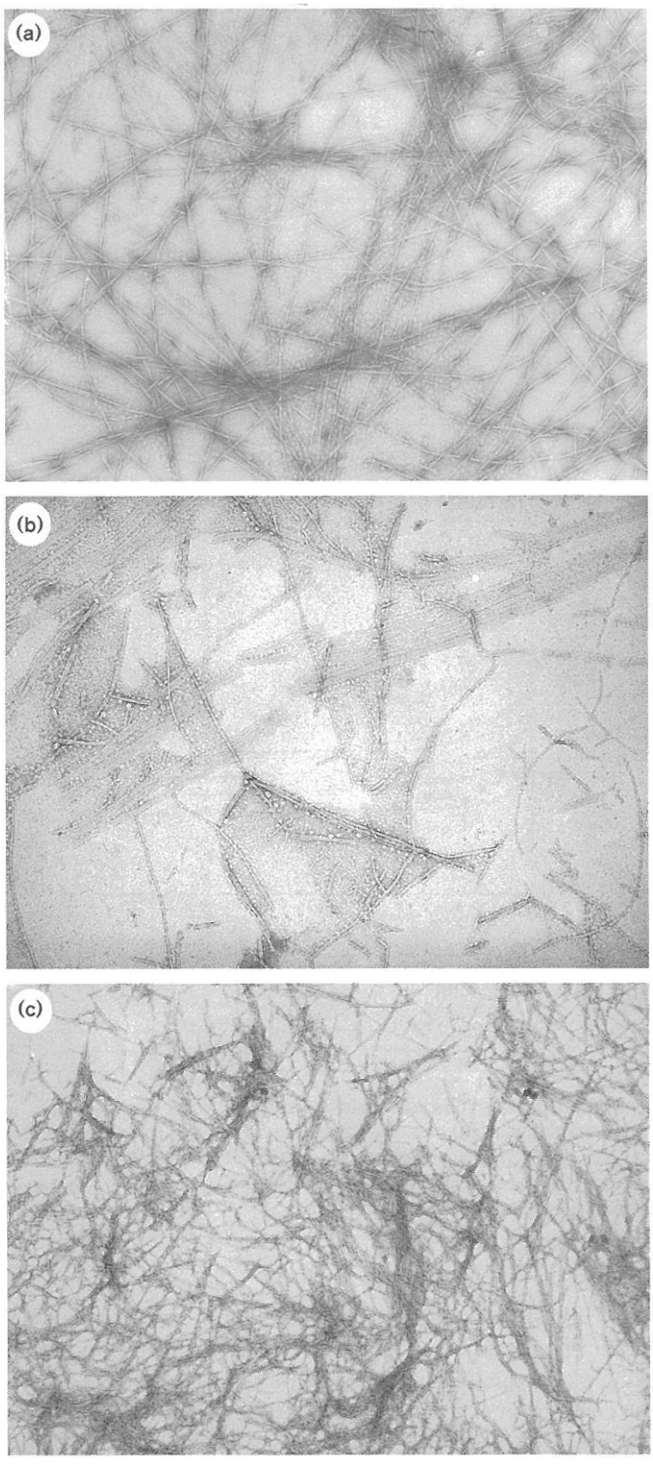

Electron micrographs of the peptides **(a)** AGAAAAGA [PrP(113–120)], **(b)** AGAACAGA [PrP(113–120)–5] and **(c)** spin-labeled AGAACAGA [PrP(113–120)–5SL]. All three peptides form fibrils.

Figure 2

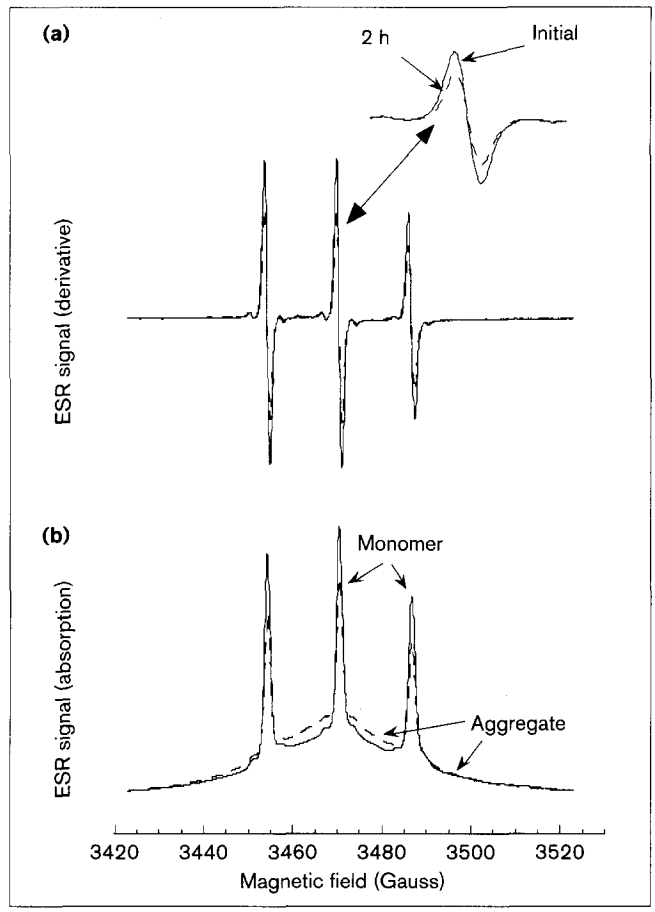

ESR spectra of PrP(113–120)–5SL in solution at the beginning of a kinetic trial (solid line) and after 2 h (dashed line). **(a)** The conventional first-derivative ESR display with the center line expanded to show the loss of signal intensity after 2 h. **(b)** The integrated signal showing the absorption spectrum. The broad background associated with aggregate is apparent under the sharp three-line spectrum.

completely removes this broad signal, indicating that this spectral feature arises from a high molecular weight peptide aggregate. Support for this interpretation comes from the shape of the broad spectrum. In solid and solid-like materials containing nitroxides, electron spin–spin exchange interactions influence the shape of the ESR spectrum. If the concentration is high, such as for polycrystalline nitroxide solids or highly concentrated solutions, the spin–spin interaction leads to exchange narrowing and an ESR spectrum containing a single Lorentzian shaped line [25,26]. The broad spectral component from the PrP(113–120)–5SL aggregate fits well to a Lorentzian function and the width at half height is ~33 Gauss, which is similar to that observed for unordered tempone microcrystals.

The concentrations of peptide in the aggregate and monomeric forms were determined at the beginning of each kinetic trial. Figure 3 shows how the concentrations of these two species depend upon total initial peptide concentration. The solid lines are linear least-squares fits

Figure 3

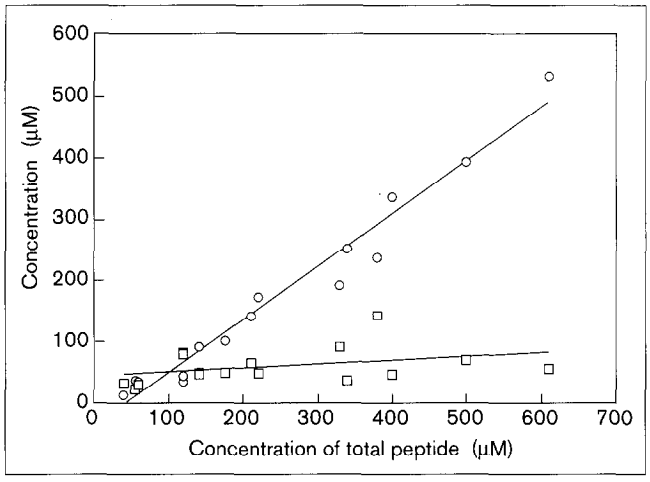

Concentrations of the PrP(113–120)–5SL peptide in the monomeric form (squares) and as aggregate (circles) plotted against total peptide concentration as determined at the beginning of each trial.

to the data. The initial aggregate concentration correlates linearly to total peptide concentration. The x intercept (zero aggregate concentration) is $51 \pm 35\,\mu M$. Thus, when the total peptide present is less than ~50 μM, all of the peptide will exist as monomer that is free in solution. Figure 3 shows that the resultant monomer concentration varies from 23 μM to 143 μM and shows little correlation to total peptide concentration.

Kinetic experiments were performed by recording spectra as a function of time. The time-dependent monomer concentration was followed using the peak-to-peak amplitude of the first derivative centerline where the aggregate derivative signal makes a negligible contribution to the amplitude of the derivative spectrum. We examined 32 samples of various total peptide concentration. Half of the samples (16/32) showed no change in the monomer signal during the initial 3 h, regardless of total peptide concentration (which ranged from approximately 10 μM to 175 μM). A common feature of these samples is that none of them contained ESR-detectable aggregate. Of the 16 samples that did exhibit a change in monomer concentration during the initial 3 h, all contained aggregate. The first 3 h of these 16 kinetic trials are shown in Figure 4. Each trial reveals an initial decay within the first 0.5–1.0 h followed by a more gradual decay that continues for two weeks (see below).

As the ESR signal that is associated with free PrP(113–120)–5SL decays, the aggregate signal correspondingly grows, as shown for one trial in Figure 5a. Quantitative absorption signal integration demonstrates that the sum of the free PrP(113–120)–5SL concentration and the aggregate concentration is approximately constant during the kinetic trials to within experimental error. Thus,

Figure 4

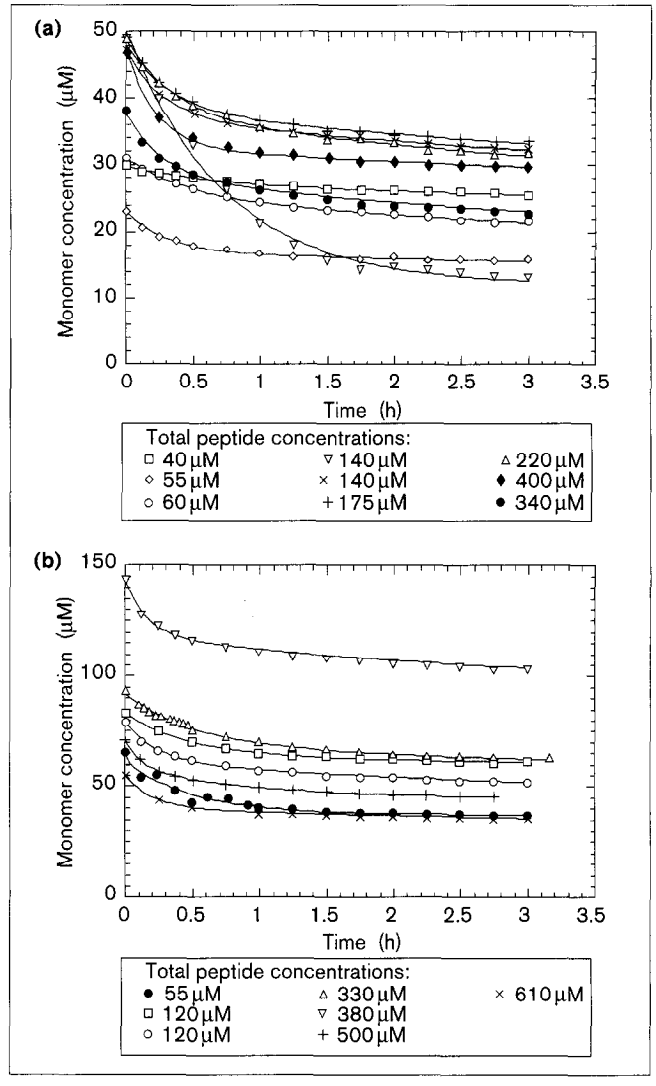

The first 3 h of the 16 kinetic trials observed for PrP(113–120)–5SL. Trials starting with **(a)** monomer less than 50 μM and **(b)** monomer greater than 50 μM are separated for clarity. Each trial exhibits an initial exponential decay within the first hour. There is no evidence of a lag period. Solid lines are fits to equation 1.

the ESR signal represents all the peptide present in solution. The disappearance of the monomer is not due to settling or destruction of the spin label but, instead, is caused by conversion of the free peptide to a solid-like form.

ESR may also be used to determine whether the peptide is oligomerizing in solution. The width of the narrow line that is associated with the free peptide is approximately proportional to the peptide rotational correlation time [24,27]. Thus, monodisperse peptide dimers or trimers, for example, would give spectral lines that are two or three times broader, respectively, than those for the monomer. A convenient way to determine if there is significant

Figure 5

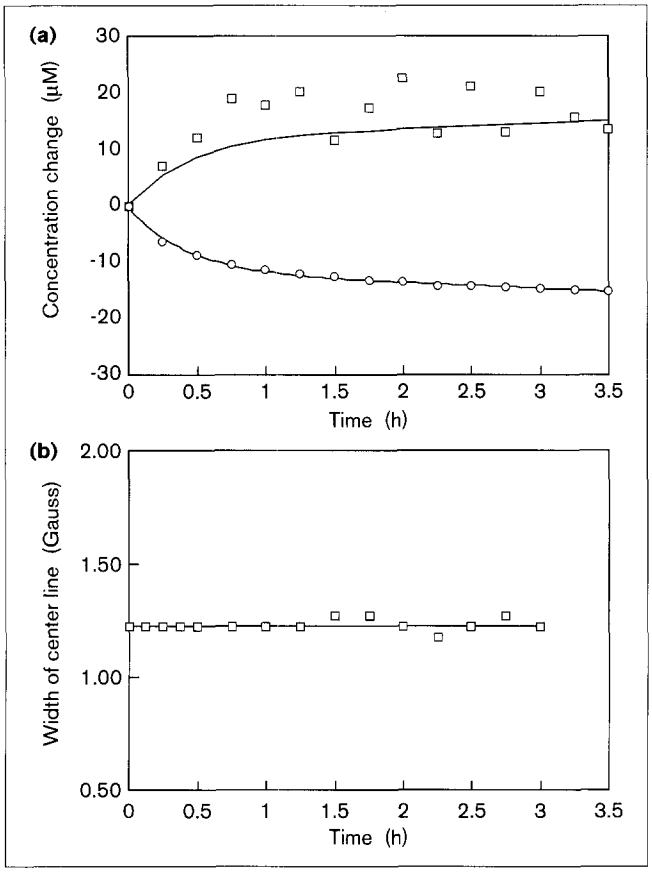

Time-dependent characteristics of the ESR signal. **(a)** The time-dependent changes in concentration of the monomer (circles) and the aggregate (squares), showing that as the monomer concentration decreases the aggregate concentration increases. The line is fitted to the monomer signal and then reflected about the $y = 0$ line to show that it approximately describes the growth of the aggregate concentration. To within experimental error, loss of monomer is compensated by growth of aggregate. **(b)** The time-dependent line width of the monomer signal. To within experimental error, the width is constant indicating that ESR does not detect dimers, trimers or other low molecular weight oligomers.

Figure 6

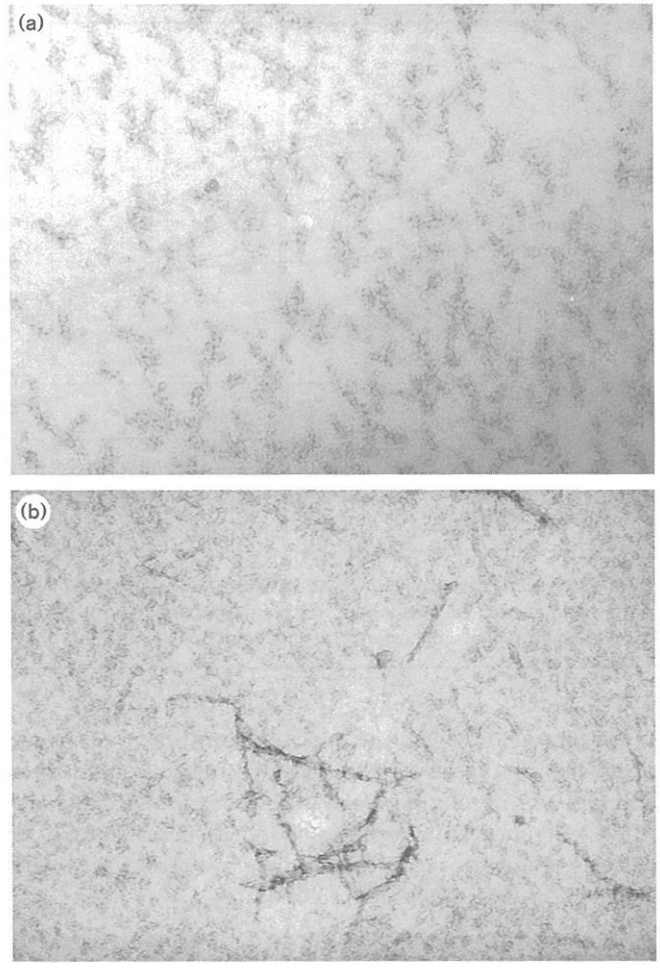

Electron micrographs of PrP(113–120)–5SL obtained **(a)** immediately after dissolution and **(b)** after 1 h. The micrograph in (a) shows only unstructured aggregates of peptide. Fibrils were not found in any samples that were dried down immediately after dissolution. In contrast, (b) shows the emergence of fibrillar structures.

oligomerization is to examine the line width of the central peak as a function of time, as shown in Figure 5b. There is no line width variation, to within experimental error, indicating that the only ESR-detectable species in solution is the peptide monomer. But the existence of small populations (<5%) of higher oligomers in a solution of mainly monomers cannot be ruled out.

EM detects two aggregate species: amorphous aggregate and amyloid

EM was employed to determine the nature of the aggregated species. Samples were prepared using the same methods used for the ESR experiments. At various times after dissolution, samples were dried on EM grids and stained as described above. Distinct time-dependent morphological stages were observed (Figure 6). Micrographs taken at time = zero reveal a rough surface that apparently contains amorphous aggregates of peptide. These aggregates do not contain the regular extended fibrillar structure associated with amyloid. At least five different samples were carefully examined and none of them contained evidence for fibrillar structures. As a control, a soluble spin-labeled peptide [28] with the following sequence — Ac-AAAAKAACA-KAAAAKA-NH_2 3K–8 — was dried on a grid and treated to the same staining procedure used for the PrP peptides. Careful examination by EM did not reveal the amorphous aggregate (as seen in Figure 6) or amyloid (Figure 1).

At 1.0–2.5 h after dissolution, EM of PrP(113–120)–5SL revealed short fibril-like structures along with the amorphous aggregate. Typically, fibrils appeared to be connected

Figure 7

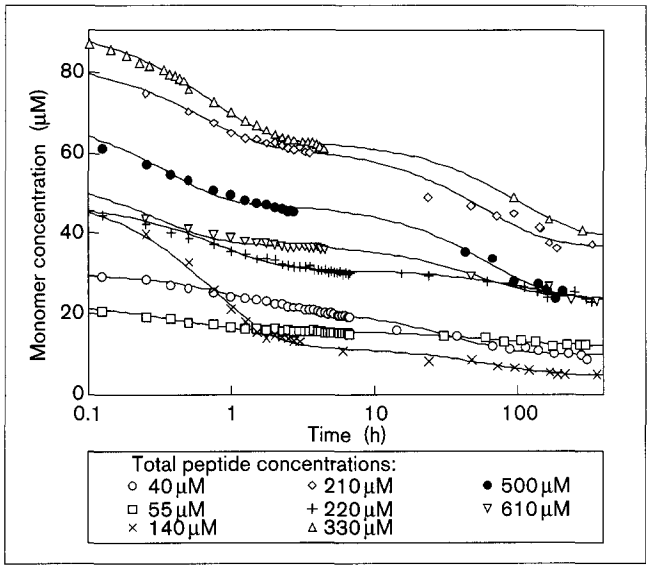

Kinetic trials of eight samples followed for up to 15 days plotted semilogarithmically. The solid lines, which are fits to equation 1, reveal the double exponential behavior of the monomer uptake.

to the amorphous aggregate and no short fibrils were found in regions that lacked amorphous aggregate. Finally, after several hours in solution, there were collections of full-sized fibrils (Figure 1). In samples that had been filtered to remove aggregate, no amorphous aggregate or fibrils were observed by EM after 18h in solution.

Characterizing the kinetics of amyloid formation

ESR distinguishes peptide that is free in solution from aggregate. Furthermore, the ESR spectra suggest that, within the detection limit of ESR, the only nonaggregated solution species is monomeric PrP(113–120)–5SL peptide. Complementary EM experiments reveal two distinct aggregate species: amorphous aggregate and amyloid. Combining the two techniques allows us to probe the interconversion among these three distinct species. At the outset, amorphous aggregate and free peptide are present. These two species decline, and fibrils are observed; filtering experiments suggest that fibril growth requires the presence of amorphous aggregate.

Of the 16 kinetic trials that showed a decrease in the monomer concentration, eight trials were allowed to proceed with periodic monitoring for up to 15 days (shown as a semilog plot in Figure 7). After the initial decay (Figure 4), the monomer peptide signal continued to decay although at a much slower rate. The position of the sample in the ESR cavity was varied to determine whether the slow decay was a consequence of peptide amorphous aggregate and/or amyloid settling in the sample tube. The concentration of total aggregate (amorphous aggregate and amyloid) was constant throughout the ESR sample, indicating that settling was not responsible for the observed slow decay and that, in contrast, the solution peptide continued to convert to an aggregate species.

ESR first derivative peak-to-peak heights (Figures 4,7) were fitted to the double exponential function:

$$\frac{[\text{monomer}]_t}{[\text{monomer}]_0} = \alpha e^{-\lambda_1 t} + \beta e^{-\lambda_2 t} + \gamma \qquad (1)$$

where λ_1 describes the initial decay and λ_2 describes the slow decay. The fits are shown as solid lines in Figures 4 and 7. While there is some scatter, in general equation 1 provides a good fit for most of the experimental data. λ_1 ranges from $1.1\,h^{-1}$ to $8.8\,h^{-1}$ (corresponding to time constants λ_1^{-1} from 0.9h to 0.1h) and λ_2 ranges from $0.007\,h^{-1}$ to $0.025\,h^{-1}$ (143h to 40h).

To elucidate the features of a kinetic model, it is important to determine how the various fitting parameters (α, λ_1, etc.) depend upon peptide and aggregate concentration. This is typically achieved in conventional homogeneous kinetics studies by varying the concentration of a single chemical species while holding constant the concentrations of all other species. Because we are examining a heterogeneous material that only partially dissolves, however, it is difficult to exert detailed control over how the total peptide partitions between amorphous aggregate and free solution peptide. To address this difficulty we used multiple linear regression [29,30]. Each parameter in equation 1 was simultaneously regressed against the initial concentrations of amorphous aggregate and monomer peptide. To within experimental error, α, β, γ and λ_2 showed no systematic variation with respect to the concentrations of amorphous aggregate or monomer peptide. But the λ_1 parameter did reveal a dependence on the amorphous aggregate concentration (Figure 8). The slope and intercept are $(7.9\pm2.3)\times10^{-3}\,h^{-1}\,\mu M^{-1}$ and $1.7\pm0.68\,h^{-1}$, respectively. There is a high level of scatter as indicated by an R^2 statistic of 0.47, so this correlation is tentative.

Figures 2, 4 and 7 clearly show that the concentration of monomer peptide decreases monotonically through each kinetic trial. To elucidate further the kinetic process leading to fibril formation, it is important to know whether amorphous aggregate and/or fibril can release monomer back to solution. A kinetic trial was initiated and allowed to run for six days. The resulting sample was filtered (0.22μm) to separate amorphous aggregate and fibril from monomeric peptide. The solid was redissolved and the concentration monitored by ESR. The result is shown in Figure 9. The data show an increase in monomer concentration indicating the release of free monomer from the solid species. Equation 1 was fitted to the data (solid line)

Figure 8

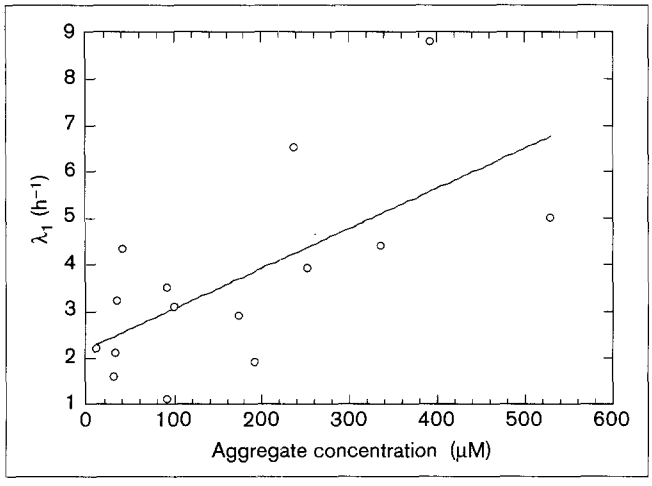

Correlation of λ_1 (equation 1) to aggregate concentration. The line represents the linear fit with slope and intercept: $(7.9 \pm 2.3) \times 10^3\ h^{-1}\ \mu M^{-1}$ and $1.7 \pm 0.68\ h^{-1}$, respectively.

Figure 9

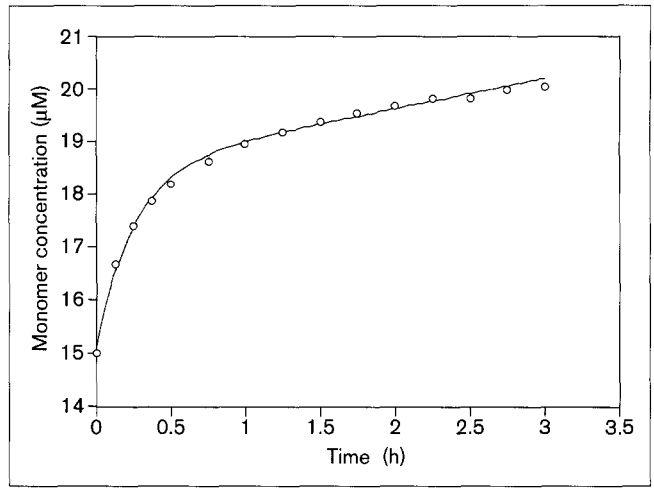

Release of monomer from redissolved filtered aggregate. The value of λ_1 obtained from the fit (solid line) is comparable to values obtained from the experiments shown in Figure 4.

and the resulting value for λ_1 was within the range of values obtained from the experiments shown in Figure 4.

Summary of experimental results and proposal of a kinetic model for the early kinetic phase

The data presented here, indicate that the spin-labeled PrP(113–120)–5 sequence forms amyloid that is similar to the parent peptide sequence. ESR detects two distinct signals: one associated with monomer PrP(113–120)–5SL and the other with aggregate. EM suggests that the aggregate is composed of amyloid and an unstructured amorphous aggregate. Inspection of micrographs obtained within the first 2 h shows that fibrils are found near amorphous aggregate. Parallel ESR and EM experiments suggest that only amorphous aggregate and monomer are present at the outset of each kinetic trial. In addition, filtering the amorphous aggregate eliminates both the ESR-detected kinetic decay observed for the monomer and EM-detected formation of fibril. In kinetic trials, the monomer peptide concentration decays for two weeks (when kinetic trials were typically terminated) and the resulting time-dependence follows a double exponential function (equation 1). The observed rate for the initial decay is ~3–5 h^{-1} and depends on the concentration of amorphous aggregate. EM reveals that short fibrils form within the same time period. Samples filtered to remove the monomer reveal that monomer is released back to solution from amorphous aggregate and/or fibril.

The kinetic data suggest that amorphous aggregate is required for the formation of fibril. Monomer in the presence of amorphous aggregate begins to decay within the dead time of each kinetic trial (~5 min). The uptake of monomer is concomitant with fibril formation and the observed rate is proportional to the concentration of amorphous aggregate. Taken together, these observations suggest that fibril growth is initiated by amorphous aggregate and, perhaps, takes place on the surface of amorphous aggregate particles. To model these observations, a three-state kinetic scheme is presented in Figure 10. Amorphous aggregate is considered to be a disordered solid that provides a source of monomer peptide [31]. Monomer may only be released from sites on the amorphous aggregate surface. In turn, a certain fraction of the surface peptides on the amorphous aggregate possess the proper conformation to initiate fibril growth. Monomer peptide attaches to these specific sites leading to fibril elongation.

Release of monomer from the amorphous aggregate is characterized by the zeroth order rate constant $k_A m_A$ where k_A is the rate constant of monomer release per site and m_A is the number of sites in the sample [32]. Similarly, $k_F m_F$ characterizes the attachment rate of monomer to the m_F fibril ends in the sample. This second process is first order with respect to the concentration of monomer in the solution. Representing monomer by the symbol M, the rate law for M is given by:

$$\frac{dM}{dt} = k_A m_A - k_F m_F\, M \qquad (2)$$

The solution to equation 2 is:

$$M_t = M_{ss} + (M_0 - M_{ss}) e^{-k_F m_F t} \qquad (3)$$

where M_0 is the initial concentration of monomer and M_{ss} is the steady state concentration of monomer given by $k_A m_A / k_F m_F$.

Figure 10

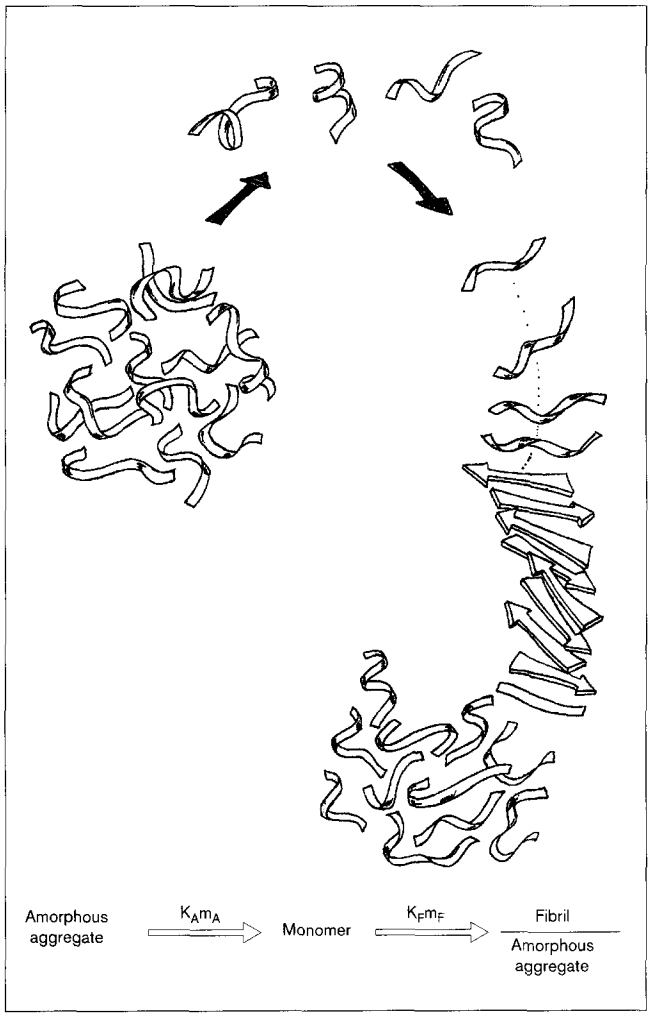

A model proposed to explain the early kinetic decay of monomer. Amorphous aggregate, which is formed at high concentration of total peptide (> 50 μM), serves as a storage pool releasing monomer to solution. The surface of amorphous aggregate also provides specific fibril initiation sites. Fibril growth sequesters monomer from solution. The kinetic behavior of this model is given by equation 3.

Equation 3 captures many of the features observed for the decay of monomer within the first several hours of each kinetic trial. The observed rate λ_1 in equation 1 is equivalent to the model value $k_F m_F$. At the outset there is a concentration of monomer that exceeds M_{ss}. This excess decays exponentially according to the rate constant $k_F m_F$. After this initial decay, the release of monomer by amorphous aggregate is balanced by the uptake of monomer as the fibrils elongate and the monomer concentration achieves a steady state. Because fibril formation takes place on the surface of amorphous aggregate, m_F should depend on the amorphous aggregate concentration. Thus, the initial decay should vary in proportion to the concentration of amorphous aggregate which is experimentally observed (Figure 8).

The proposed kinetic model does not account for the slow decay of monomer that continues after the first several hours. It is most likely that the slow decay results from the eventual loss of amorphous aggregate as monomer is released. This loss may be included using the *ad hoc* expression:

$$m_A = m_{A,0} e^{-k_R t} \quad (4)$$

where $m_{A,0}$ is the number of sites releasing monomer at $t = 0$ and k_R represents the rate constant for the loss of such sites as the concentration of amorphous aggregate decreases. Incorporating equation 4 into equation 2 and solving gives a double exponential decay (without an additive constant) for the decay of monomer.

It should be noted that the kinetic data presented here could be readily fitted to other kinetic models. For instance, one could propose reversible reactions between amorphous aggregate and solution monomer and between monomer and fibril. Alternatively, there could be direct reaction from amorphous aggregate to fibril arising from rearrangement of peptides on the surface of the aggregate. It is our view that the model offered above provides a good working hypothesis and is presently the simplest scheme consistent with the experimental observables.

Discussion

The experiments presented here demonstrate that a spin-labeled analog of the PrP(113–120) sequence retains the tendency to form amyloid. The kinetic uptake of the PrP(113–120)–5SL peptide is readily observed by ESR and EM detects the concomitant formation of amyloid. In addition to monomer and amyloid, these experiments suggest that amorphous aggregate plays a key role in amyloidogenesis. Amorphous aggregate has been recognized in previous works as a kinetically favored, but thermodynamically unfavored intermediate that is involved in the crystallization of globular proteins [31,33]. The conventional role for amorphous aggregate in crystallization is essentially that of a storage pool of polypeptide, but the work presented here suggests that an amorphous aggregate can have a distinct and obligatory role in amyloid formation. The lack of a lag time for monomer uptake, the correlation of λ_1 to the concentration of amorphous aggregate and the absence of amyloid formation and monomer uptake for samples lacking amorphous aggregate, all argue that an amorphous aggregate initiates amyloidogenesis. We suggest that a small fraction of the peptides on the surface of an amorphous aggregate possess the proper conformation to initiate fibril growth. Given the high β-sheet content of typical fibrils, these fibril-initiation peptides are most likely to be in an extended β-strand conformation. Monomeric peptides from solution align and attach through hydrogen bonds to these initiating peptides. This process is repeated, resulting in an extended β sheet and the formation of fibrils.

Other hypotheses regarding the process of amyloidogenesis have been presented. Lansbury and colleagues [22,34] have suggested that amyloid formation is analogous to crystal growth. Using light scattering measurements as their principal technique for monitoring amyloidogenesis, they found that supersaturated solutions exhibit a lag period before fibril is detected and, further, that the lag period can be eliminated if the sample is seeded with mature fibrils. They therefore proposed that one-dimensional crystallization, similar to the polymerization of actin and other types of protein assembly, underlies the development of amyloid. Although one-dimensional crystallization successfully explains their light scattering data, it has been noted that accumulated PrP^{Sc} in diseased animals usually lacks the long range order that characterizes fibrils [35]. In addition, Wille *et al.* [36] used fluorinated solvents to examine the importance of secondary structure in prion infectivity. By examining a proteolytic fragment of PrP [PrP(27–30)] in a range of cosolvent mixtures they demonstrated a clear separation of prion infectivity from amyloid formation.

Lomakin *et al.* [23] have used quasielastic light scattering to probe the time-dependent growth of fibrils produced from a fragment of the amyloid β-protein (1–40). They found that a critical concentration of 100 μM peptide is required for fibrilogenesis. Above this critical concentration they detected the presence of 14 nm diameter micelles and it is argued that these micelles nucleate fibril growth. In the light of this work it is worthwhile considering whether the amorphous aggregate observed for the PrP(113–120)–5SL peptide is actually peptide that is sequestered in a micellar form. Micelles are unilamellar structures, 10–20 nm across [37] that should readily pass through the 0.22 μm filters used here to separate amorphous aggregate from monomer peptide. We have found that filtered solutions do not form amyloid as detected by either ESR or EM, however. Thus, we conclude that the amorphous aggregate identified for the PrP(113–120)–5SL is a large aggregate and probably not a micellar structure.

The intermediate role of the amorphous aggregate in promoting amyloidogenesis is a new hypothesis that may lead to a clearer understanding of the conversion of PrP^{C} to PrP^{Sc} and the subsequent formation of amyloid under some conditions. In contrast to the fibrillogenic theories outlined above, the conversion of PrP^{C} to PrP^{Sc} is thought to take place through specific contacts within individual PrP^{Sc}–PrP^{C} complexes. The mechanism that stabilizes PrP in the scrapie form, thereby halting reversion back to PrP^{C}, has yet to be identified, however.

It has been noted that PrP^{Sc} often accumulates as amorphous aggregates upon purification. In addition, recent work suggests that aggregates of PrP^{Sc} can bind PrP^{C}, sequestering it in a proteinase-K-resistant form [38]. The findings presented here suggest that the surface of an amorphous aggregate may promote formation of amyloid in a PrP-derived peptide. It is well established that PrP^{Sc} is rich in β sheet [7,8,36] and recent work suggests that nonfibrillar protein aggregates such as inclusion bodies may contain high levels of β sheet (A.L. Fink, personal communication). Thus, fibril-forming peptides may bind to the surface of amorphous aggregates via contacts similar to those that link adjacent strands in protein β sheets. For the prion protein, accumulation of PrP^{Sc} as amorphous aggregates helps stabilize the putative β-sheet region of PrP^{Sc} without any need for the formation of amyloid.

Conclusion

We have demonstrated that a spin-labeled PrP-derived peptide forms amyloid. When dissolved in aqueous solution, the amplitude of the ESR spectrum of the peptide is time-dependent, indicating the uptake of monomer peptide as amyloid is formed. Probing the details of monomer uptake along with parallel EM studies suggest that amorphous aggregate is responsible for initiating fibril formation. It is possible that amorphous aggregate of PrP plays an analogous role in the conversion of PrP^{C} to PrP^{Sc}. The ESR methods developed here should readily extend to other peptides and proteins that form amyloid.

Significance

The scrapie form of the prion protein is thought to be responsible for the transmission of prion diseases such as scrapie, bovine spongioform encephalopathy and Creutzfeldt–Jakob disease. Fragments of the prion protein can assemble into amyloid, but little is known about the kinetics and mechanism of amyloid formation. Here, we have used electron spin resonance and electron microscopy to show that a spin-labeled prion-derived peptide forms amyloid. Peptide monomer levels decrease as amyloid forms, and our results suggest that the formation of an amorphous peptide aggregate that is devoid of fibrils is required for fibril formation, and that the aggregate also releases peptide monomer into solution. The techniques developed in this study may prove useful in investigations of other systems in which amyloid is formed.

Materials and methods

Peptide synthesis, purification, and spin labeling

The peptides were synthesized by Fmoc solid-phase peptide synthesis on a Rainin PS3 peptide synthesizer with the carboxy-terminal alanine linked to *p*-benzyloxybenzyl alcohol (Wang) resin (Novabiochem, La Jolla, CA, USA). From residues four through seven, unreacted additions were capped with acetic anhydride (Fisher). All couplings were allowed to react for 100 min. The peptides were then cleaved with 90% trifluoroacetic acid (TFA) / 5% triethylsilane / 5% anisole (Pierce, Rockford, IL, USA / Aldrich Chemical Co., Milwaukee, WI, USA / Aldrich). The trifluoroacetic acid was distilled off under high vacuum, and the peptide precipitated with *t*-butyl methyl ether (Aldrich). About 1 mg of crude peptide was dissolved in 50 μl trifluoroethanol (Aldrich) without aggregation. The volume of the sample was brought up to 1.0 ml with 0.1% TFA buffer pH 2.6 and immediately was injected into a HPLC fitted with an analytical C18 column (Alltech, Deerfield, IL, USA). Separation of the

unlabeled peptide was obtained with a binary water (pH 2.6) and acetonitrile (Fisher) gradient, where the acetonitrile proportion increased from 5% to 55% over 50 min. Both solvents had 0.1% TFA as an ion-pairing reagent, and the total flow rate was 0.5 ml/min. The collected fractions were then dried under vacuum and stored at −10°C. The peptide was reconstituted in 50 μl acetonitrile and reacted with a ten-fold excess of methanethiosulfonate spin label (MTSSL, Reanal, Hungary) for 2 h. The resulting spin-labeled peptide was again purified by reverse phase HPLC, and just prior to injection the sample was brought up to 1.0 ml with 5% acetonitrile / 0.1% aqueous TFA (pH 2.6) solution. The labeled peptide fraction was collected and dried under vacuum. The molecular weights of the unlabeled and labeled peptides were verified by fast atom bombardment mass spectrometry and agreed with the expected values to within 1 atomic mass unit.

Centrifugal microfilters (Alltech, 0.22 μm) were used to collect amyloid and amorphous aggregate. These samples were spun in a Fisher microcentrifuge for 1 min. The solid material retained on the filter was put in contact with fresh buffer solution by placing the filter in new buffer and vortexing for 20 s.

Electron spin resonance

The dry purified spin-labeled peptide sample was placed in a click top tube containing 30–50 μl of buffer (0.1 M sodium acetate pH 5.5, hereafter referred to as the standard buffer). The solution and peptide pellet were agitated with the plastic tip of the pipette for 10 s. The solution was then vortexed for 10 s and centrifuged for 5 s to break down the resultant foam. The solution was then drawn into a 100 μl capillary tube and flame sealed at both ends. The ESR measurements were begun within 5 min following reconstitution in the buffer.

Continuous wave ESR spectra of the spin-labeled peptides were acquired on a Bruker ESP 380 equipped with a dielectric resonator. The dielectric resonator was used due to its increased sensitivity, approximately a factor of five over the standard TE_{102} resonator. Peptide concentrations down to 10 μM were readily detected. Temperature control was maintained at 298K with a Bruker variable temperature unit. Concentrations were determined by double integration of the ESR spectra followed by quantitative comparison to a 1.0 mM 4-hydroxy-TEMPO (Aldrich) standard solution. The modulation frequency was 100 kHz, and the amplitude was 0.66 G. Spectra were gathered over a 100 G scan width.

During kinetic trials, spectra were obtained every 7.5 min for the first 30 min, and every 15 min thereafter for 3 h. For eight samples, spectra were acquired every 24 h for up to two weeks.

To determine the aggregate concentration, a background function representing the aggregate was constructed from the difference of two experimental spectra – one at low concentration (40 μM) containing no aggregate background and one at high concentration spectrum (610 μM) containing a large aggregate background. The broad singlet background gave an observed 33 G (FWHH) singlet. This signal was integrated and scaled to all the time=0 absorption spectra to derive initial aggregate concentrations. The fit was then subtracted from the original spectra, resulting in a monomer signal which was integrated (and compared to the tempol standard) to obtain the initial monomer concentrations.

Transmission electron microscopy

Sample grids were prepared by dipping a Gold-Seal glass slide into a 1% Formvar solution. The films were floated off in nanopure water and picked up on copper 300 mesh grids. Aliquots (5 μl) of ~0.5 mM peptide suspensions in the standard buffer were placed on the grids, allowed to sit for 45 s, and blotted on the periphery of the sample. The sample was negatively-stained with 2% (w/v) uranyl acetate for 45 s and then again blotted. Samples were viewed with JEOL 100S and JEOL 100B electron microscopes operating at 80 kV (JEOL USA Inc., Peabody, MA, USA).

To obtain time course data, a copper grid was prepared as above immediately following dissolution in the buffer for the t=0 data, and a new grid prepared every 30 min during the course of the amyloid reaction for 4 h and again at 18 h.

Acknowledgements

The authors are grateful to Jonathan Krupp of the UCSC Electron Microscopy Facility for his help with the TEM experiments and to Eefei Chen for sketching the artwork in Figure 10. Also acknowledged are Lydia Gregoret, Tony Fink, Paul Hanson, Kim Bolin, Julie Trulson and Stephanie Corchnoy for helpful comments on the manuscript. This work was supported by NSF grant MCB 9408284 (G.L.M.) and NIH grants GM46870 (G.L.M.), GM16716 (C.J.S.) and AG02132 (S.B.P., F.E.C.).

References

1. Prusiner, S.B. (1995). The prion diseases. *Scientific American* **272**, 48–57.
2. Cohen, F.E., Pan, K.M., Huang, Z., Baldwin, M., Fletterick, R.J. & Prusiner, S.B. (1994). Structural clues to prion replication. *Science* **264**, 530–531.
3. Prusiner, S.B. (1992). Chemistry and biology of prions. *Biochemistry* **31**, 12277–12288.
4. Prusiner, S.B. (1991). Molecular biology of prion diseases. *Science* **252**, 1515–1522.
5. Prusiner, S.B., *et al.*, & Dearmond, S.J. (1990). Transgenetic studies implicate interactions between homologous prp isoforms in scrapie prion replication. *Cell* **63**, 673–686.
6. Telling, G.C., *et al.*, & Prusiner, S.B. (1996). Evidence for the conformation of the pathologic isoform of the prion protein enciphering and propagating prion diversity. *Science* **274**, 2079–2082.
7. Caughey, B.W., Dong, A., Bhat, K.S., Ernst, D., Hayes, S.F. & Caughey, W.S. (1991). Secondary structure analysis of the scrapie-associated protein prp 27-30 in water by infrared spectroscopy. *Biochemistry* **30**, 7672–7680.
8. Pan, K.M., *et al.*, & Prusiner, S.B. (1993). Conversion of α-helices into β-sheets features in the formation of the scrapie prion proteins. *Proc. Natl Acad. Sci. USA* **90**, 10962–10966.
9. Safar, J., Roller, P.P., Gajdusek, D.C. & Gibbs, C.J., Jr. (1993). Conformational transitions, dissociation, and unfolding of scrapie amyloid (prion) protein. *J. Biol. Chem.* **268**, 20276–20284.
10. Zhang, H., *et al.*, & Prusiner, S.B. (1995). Conformational transitions in peptides containing two putative alpha-helices of the prion protein. *J. Mol. Biol.* **250**, 514–526.
11. Heller, J., *et al.*, & Wemmer, D.E. (1996). Solid-state nmr studies of the prion protein h1 fragment. *Protein Sci.* **5**, 1655–1661.
12. Huang, Z.W., Gabriel, J.M., Baldwin, M.A., Fletterick, R.J., Prusiner, S.B. & Cohen, F.E. (1994). Proposed three-dimensional structure for the cellular prior protein. *Proc. Natl Acad. Sci. USA* **91**, 7139–7143.
13. Riek, R., Hornemann, S., Wider, G., Billeter, M., Glockshuber, R. & Wuthrich, K. (1996). NMR structure of the mouse prion protein domain PrP(121–321). *Nature* **382**, 180–182.
14. Gasset, M., *et al.*, & Prusiner, S.B. (1992). Predicted alpha-helical regions of the prion protein when synthesized as peptides form amyloid. *Proc. Natl Acad. Sci. USA* **89**, 10940–10944.
15. Schatzl, H.M., Da Costa, M., Taylor, L., Cohen, F.E. & Prusiner, S.B. (1995). Prion protein gene variation among primates. *J. Mol. Biol.* **245**, 362–374.
16. Dohura, K., Tateishi, J., Sasaki, H., Kitamoto, T. & Sakaki, Y. (1989). Pro → Leu change at position-102 of prion protein is the most common but not the sole mutation related to Gerstmannstraussler syndrome. *Biochem. Biophys. Res. Commun.* **163**, 974–979.
17. Huang, Z., Prusiner, S.B. & Cohen, F.E. (1996). Scrapie prions: a three-dimensional model of an infectious fragment. *Fold. Des.* **1**, 13–19.
18. Glenner, G.G., Eanes, E.D. & Page, D.L. (1972). The relation of the properties of congo red-stained amyloid fibrils to the β conformation. *J. Histochem. Cytochem.* **20**, 821–826.
19. Prusiner, S.B., *et al.*, & Glenner, G.G. (1983). Scrapie prions aggregate to form amyloid-like birefringent rods. *Cell* **35**, 349–358.
20. DeArmond, S.J., McKinley, M.P., Barry, R.A., Braunfeld, M.B., McColloch, J.R. & Prusiner, S.B. (1985). Identification of prion amyloid filaments in scrapie-infected brain. *Cell* **41**, 221–235.

21. Wisniewski, T., Ghiso, J. & Frangione, B. (1991). Peptides homologous to the amyloid protein of Alzheimer's disease containing a glutamine for glutamic acid substitution have accelerated amyloid fibril formation. *Biochem. Biophys. Res. Commun.* **179**, 1247–1254.
22. Come, J.H., Fraser, P.E. & Lansbury, P.T. (1993). A kinetic model for amyloid formation in the prion diseases - importance of seeding. *Proc. Natl Acad. Sci. USA* **90**, 5959–5963.
23. Lomakin, A., Chung, D.S., Benedek, G.B., Kirschner, D.A. & Teplow, D.B. (1996). On the nucleation and growth of amyloid beta-protein fibrils - detection of nuclei and quantitation of rate constants. *Proc. Natl Acad. Sci. USA* **93**, 1125–1129.
24. Todd, A.P. & Millhauser, G.L. (1991). ESR spectra reflect local and global mobility in a short spin-labeled peptide throughout the α-helix→coil transition. *Biochemistry* **30**, 5515–5523.
25. Poole, C.P. & Farach, H.A. (1971). *Relaxation in Magnetic Resonance.* Academic Press, New York, USA.
26. Wertz, J.E. & Bolton, J.R. (1986) *Electron Spin Resonance: Elementary Theory and Practical Applications.* Chapman and Hall, New York, USA.
27. Berliner, L.J. (1976). *Spin Labeling: Theory and Applications.* Academic Press, New York, USA.
28. Miick, S.M., Todd, A.P. & Millhauser, G.L. (1991). Position dependent local motions in spin-labeled analogues of a short α helical peptide determined by electron spin resonance. *Biochemistry* **30**, 9498–9503.
29. Press, W.H., Flannery, B.P., Teukolsky, S.A. & Vetterling, W.T. (1986). *Numerical Recipes: The Art of Scientific Computing.* Cambridge University Press, Cambridge, UK.
30. Bevington, P.R. (1969). *Data Reduction and Error Analysis for the Physical Sciences.* McGraw-Hill, New York, USA.
31. De Young, L.R., Fink, A.L. & Dill, K.A. (1993). Aggregation of globular proteins. *Accts Chem. Res.* **26**, 614–620.
32. Walton, A.G. (1967). *The Formation and Properties of Precipitates.* Wiley, New York. USA.
33. Feher, G. & Kam, Z. (1985). Nucleation and growth of protein crystals: general principles and assays. *Methods Enzymol.* **114**, 77–112.
34. Jarrett, J.T. & Lansbury, P.T. (1993). Seeding one dimensional crystallization of amyloid - a pathogenic mechanism in Alzheimer's disease and scrapie. *Cell* **73**, 1055–1058.
35. Mckinley, M.P., *et al.*, & Prusiner, S.B. (1991). Scrapie prion rod formation in vitro requires both detergent extraction and limited proteolysis. *J. Virology* **65**, 1340–1351.
36. Wille, H., Zhang, G.F., Baldwin, M.A., Cohen, F.E. & Prusiner, S.B. (1996). Separation of scrapie prion infectivity from PrP amyloid polymers. *J. Mol. Biol.* **259**, 608–621.
37. Cantor, C.R. & Schimmel, P.R. (1980). *Biophysical Chemistry, Volumes I, II and III.* W. H. Freeman, San Francisco, USA.
38. Caughey, B., Kocisko, D.A., Raymond, G.J. & Lansbury, P.T. (1995). Aggregates of scrapie-associated prion protein induce the cell-free conversion of protease-sensitive prion protein to the protease-resistant state. *Chem. Biol.* **2**, 807–817.